Author's Accepted Manuscript

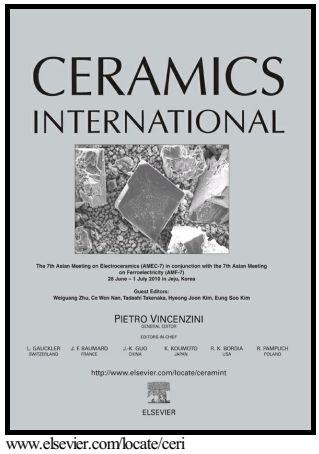

www.elsevier.com/locate/ceri

A Study of the Structural and Morphological Properties of Ni–Ferrite, Zn–Ferrite and Ni–Zn–Ferrites Functionalized with Starch

Ljubica Andjelković, Marija Šuljagić, Mladen Lakić, Dejan Jeremić, Predrag Vulić, Aleksandar S. Nikolić

PII: S0272-8842(18)31149-0
DOI: https://doi.org/10.1016/j.ceramint.2018.05.018
Reference: CERI18193

To appear in: *Ceramics International*

Received date: 2 April 2018
Revised date: 3 May 2018
Accepted date: 3 May 2018

Cite this article as: Ljubica Andjelković, Marija Šuljagić, Mladen Lakić, Dejan Jeremić, Predrag Vulić and Aleksandar S. Nikolić, A Study of the Structural and Morphological Properties of Ni–Ferrite, Zn–Ferrite and Ni–Zn–Ferrites Functionalized with Starch, *Ceramics International,* https://doi.org/10.1016/j.ceramint.2018.05.018

A Study of the Structural and Morphological Properties of Ni–Ferrite, Zn–Ferrite and Ni–Zn–Ferrites Functionalized with Starch

Ljubica Andjelković[1*], Marija Šuljagić[2], Mladen Lakić[3], Dejan Jeremić[3], Predrag Vulić[4], Aleksandar S. Nikolić[2*]

[1]Department of Chemistry, IChTM, University of Belgrade, Studentski Trg 12–16, 11000 Belgrade, Serbia

[2]Faculty of Chemistry, University of Belgrade, Studentski Trg 12–16, 11000 Belgrade, Serbia

[3]Innovation Center of the Faculty of Chemistry, University of Belgrade, Studentski Trg 12–16, 11000 Belgrade, Serbia

[4]Faculty of Mining and Geology, University of Belgrade, Djušina 7, 11000 Belgrade, Serbia

[*]Corresponding authors:

ljubica@chem.bg.ac.rs

asn@chem.bg.ac.rs

Abstract

Zinc–ferrite, nickel–ferrite and mixed nickel–zinc ferrites were successfully synthesized *via* the thermal decomposition method from acetylacetonate complexes. To control the particle size and enhance dispersibility in an aqueous medium, starch, a natural and biocompatible compound, was used for the first time for coating such magnetic powders. X-ray powder diffraction (XRPD) was performed to study the structural properties of all samples. The presence of a single-phase spinel structure as well as the cation distribution in both sites of all investigated magnetic powders was confirmed. The values of unit cell parameters obtained from the results of the Rietveld analysis decreased, while the average crystallite size increased with increasing Ni^{2+} content. The average microstrain parameters unambiguously showed a change in the spinel structure with cation distribution. Scanning electron

microscopy (SEM), energy-dispersive X-ray spectroscopy (EDS) and Fourier transform infrared spectroscopy (FTIR) analyses were also utilized to characterize the synthesized materials, corroborating the XRPD data. The obtained results indicated that functionalization by starch was successfully achieved.

Keywords: Ferrites, Powders, Solid state reaction, Functionalization, Structural properties

1. Introduction

Ferrimagnetic oxides, or ferrites, are very attractive materials due to their outstanding physical properties and high applicability in nanotechnology [1]. For example, they are widely utilized as industrial ceramics where nanomaterials with improved performances are required. Nickel ferrite ($NiFe_2O_4$) finds numerous technological applications, such as gas-sensor [2,3], magnetic fluids [4], catalysts [5–7], photomagnetic materials [8] and microwave devices [9]. Zinc ferrite ($ZnFe_2O_4$) has more specific applications, including as a promising semiconductor photocatalyst [10,11], photo-induced electron transfer [12], photoelectrochemical cells [13] and photochemical hydrogen production [14,15]. Mixed nickel–zinc ferrites are widely used in electromagnetic applications where a high permeability is required, such as inductors [16] and electromagnetic wave absorbers [17–20]. Currently, besides technical usage, there is a growing interest in the medical application of these materials in diagnostics and therapy, encompassing magnetic resonance imaging (MRI) [21–23], hyperthermia [24–27], and so forth [28–32].

The magnetic properties of ferrites are tightly bound to the position of the divalent cations in the crystal structure. Ferrites crystallize in a spinel structure (cubic space group $Fm\bar{3}d$), where divalent and trivalent cations are arranged among tetrahedral and octahedral

sites. Magnetic divalent cations (Ni^{2+}) have strong preference for the octahedral sites, and thus, $NiFe_2O_4$ is an inverse spinel. In contrast, diamagnetic divalent cations, such as Zn^{2+}, occupy tetrahedral sites. Therefore, the structure of $ZnFe_2O_4$ is a normal spinel. Due to the opposite path of crystallization, the properties of $NiFe_2O_4$ and $ZnFe_2O_4$ are diametrically different, *i.e.*, $NiFe_2O_4$ is ferrimagnetic with a Curie temperature ≈ 858 K, while $ZnFe_2O_4$ shows antiferromagnetic ordering below 9 K. The composition of a ferrite can be modified, while the basic crystalline structure remains the same, meaning that the properties of materials can be easily tuned just by varying the ratio of the divalent cations. Mixed nickel–zinc ferrites has the general site occupancy $(Zn_xFe_{1-x})_{TET}[Ni_{1-x}Fe_{1+x}]_{OCT}O_4$, where the composition varies from $NiFe_2O_4$ (x = 0) to $ZnFe_2O_4$ (x = 1), resulting in the redistribution of metal ions over the tetrahedral and octahedral sites and modification of the properties.

Preparation methodology is essential for controlling the physical properties of the materials, such as magnetic, electrical and optical properties [33]. In other words, the synthesis procedure determines the structural and microstructural characteristics of the materials, such as cation distribution, particle size, microstrain and kinds of defects [34–36]. Different methods for the synthesis of nanocrystalline ferrites have been developed in order to optimize low-cost synthesis/material with the desired characteristics ratio [33,37]. The preparation methods can be divided in two main categories, solid state and wet chemistry. One of the interesting solid state synthetic routes for the preparation of ultrafine powders is by thermal decomposition of complexes with acetylacetone ligands [38,39]. Most metals form complexes with β-diketonato ligands and the prepared complexes have relatively low temperatures of thermal decomposition (below 500 °C), although solid phase reactions mainly require high temperature sintering (1200 – 1300 °C) [40].

The biomedical application of ferrites requires controllable particle size and enhanced dispersibility in a physiological medium. Surface coating of ferrites with a layer of

hydrophilic molecules or polymers improves biocompatibility and the stability of the colloid. Moreover, interaction with various biological entities, such as polypeptide, antibodies, enzymes and DNA, becomes more effective. Besides for example citric and oleic acid [41–43], starch has become a popular surfactant in the preparation of magnetic particles for biomedical applications due to its high availability, low cost and non-toxic effects [44].

In this work, surface coating of $NiFe_2O_4$, $ZnFe_2O_4$ and mixed Ni–Zn ferrites obtained from acetylacetone complexes was achieved using starch for the first time. Investigation of their structural and microstructural properties by X-ray powder diffraction (XRPD) was performed. The determination of structure parameters, especially cation distribution, is an important prerequisite in understanding and controlling the properties of ferrite nanoparticles.

2. Materials and Methods

2.1 Synthesis of $ZnFe_2O_4$, $NiFe_2O_4$, and Ni–Zn ferrites

All of the chemicals were of reagent grade, obtained from Sigma–Aldrich, and used without further purification. $ZnFe_2O_4$, $NiFe_2O_4$, and Ni–Zn ferrites were synthesized by thermal decomposition of the appropriate complexes $[M(AA)_x]$, where M denotes the corresponding cation: Zn^{2+}, Ni^{2+}, or Fe^{3+} [38–40], and AA represents acetylacetone (2,4-pentanedione) ligand. The complexes $[M(AA)_x]$ were synthesized according to a slightly modified standard method by reaction of metal ions with ammonium acetylacetonate. The thermal decomposition of the mixture of basic complexes in stoichiometric ratio suspended in toluene was performed in an electrical furnace with a heating rate of 10 °C/min at T = 500 °C for 1 hour, followed by pulverization in an agate mortar. To obtain ferrofluids, 5 g of starch was dissolved in 100 ml of boiling water. Then, 1 g of ferrite powder was added, and the mixture was ultrasonically treated for 1 hour at 80 °C. The starch-coated ferrite particles were dialyzed at 37 °C for 24 hours under continuous stirring to remove the excess unreacted starch. The pore sizes of dialysis tubing were 10 mm flat-width (50 kD MWCO).

2.2 Characterizations

XRPD patterns for all of the samples were collected using a Rigaku SmartLab automated powder X-ray diffractometer with Cu $K\alpha_{1,2}$ (λ = 1.54059 Å) radiation (U = 40 kV, I = 30 mA) equipped with D/teX Ultra 250 stripped 1D detector in the XRF reduction mode. The diffraction angle range was 15 – 80 °2θ with a step of 0.01 ° at a scan speed of 2 °/min. Structural and microstructural investigation of all samples (ferrites and ferrites coated with starch) was conducted by the Rietveld method.

Scanning electron microscopy (SEM) and Energy-dispersive X-ray spectroscopy (EDS) analyses of the samples were performed with a JEOL JSM-6610LV scanning electron microscope. EDS analyses were conducted in the area of $1x10^4$ μm^2 per sample.

The IR spectra were recorded on a Nicolet 6700 FT-IR instrument (Thermo Scientific), in the ranges of 4000 – 400 and 700 – 240 cm^{-1} using the ATR technique with a Smart Orbit accessory (diamond crystal).

3. Results and Discussion

The obtained XRPD results were analyzed by the Rietveld method to gain deeper insight into the structural and microstructural parameters, by the fundamental parameters approach [45], as implemented in PDXL2 Rigaku software.

The powder XRD patterns for synthesized ferrites, as well as for nanoparticles coated with starch, are shown in Figure 1. The powder XRD patterns for both groups of samples showed the characteristic peaks for the spinel structure. The *d*-values and intensities of the diffraction maxima match the literature data of $ZnFe_2O_4$ (ICDD PDF 22-1012) and $NiFe_2O_4$ (10-0325). The X-ray diffraction patterns show broad peaks indicating the ultrafine nature and small crystallite size of the particles. It is important to note that no other phases were detected. The most intensive diffraction peaks that correspond to the characteristic

crystallographic planes of the spinel structure of ferrites [(111), (220), (311), (400), (511), (440)] can be seen in Figure 1.

The lattice parameters were refined for all of the compositions and are listed in Table 1. According to the results, the lattice parameters increase with increasing Zn^{2+} content. The lattice parameter of these nanoparticles depends on the radius of Zn^{2+} and Ni^{2+} ions. The radius of Zn^{2+} (0.82 Å) is larger than that of Ni^{2+} (0.78 Å). The increase in lattice parameter with decreasing Ni^{2+} content is due to the replacement of the smaller Ni^{2+} cation by the larger Zn^{2+} cation [46,47].

The values of average crystallite size and microstrain obtained by the Rietveld method are listed in Table 1, while the cation occupancy distribution is listed in Table 2. It can be noticed that the crystallite size increases with increasing concentration of Ni^{2+} ions. Coating with starch led to an increase in the crystallite size, supporting the fact that the synthesized nanoparticles were functionalized. On the other hand, the microstrain increased in both the coated and uncoated samples, until the composition of $Zn_{0.5}Ni_{0.5}Fe_2O_4$. Furthermore, with further increase in the content of Ni^{2+} ions in the structure, the microstrain parameter decreased. This could be explained by the change of the structure from normal ($ZnFe_2O_4$) to inverse ($NiFe_2O_4$) spinel. The distribution of divalent metal cations at specific tetrahedral and octahedral positions shown in Table 2 is responsible for the relaxation of the structure.

Table 1. Unit cell parameters (Å), volumes (Å^3) and microstructural parameters for the investigated ferrites

	a (Å)	*V* (Å^3)	Crystallite size (Å)	Strain (%)
$ZnFe_2O_4$	8.4390(4)	601.00(5)	141(2)	0.21(6)
$ZnFe_2O_4$*	8.4371(5)	600.60(6)	202(2)	0.251(8)
$Zn_{0.75}Ni_{0.25}Fe_2O_4$	8.4140(6)	595.68(8)	173(2)	0.366(8)
$Zn_{0.75}Ni_{0.25}Fe_2O_4$*	8.4138(6)	595.62(7)	295(5)	0.469(5)

$Zn_{0.5}Ni_{0.5}Fe_2O_4$	8.3959(6)	591.84(8)	180(2)	0.426(8)
$Zn_{0.5}Ni_{0.5}Fe_2O_4$*	8.3989(6)	592.47(7)	309(3)	0.423(6)
$Zn_{0.25}Ni_{0.75}Fe_2O_4$	8.3594(6)	584.15(7)	206(2)	0.153(7)
$Zn_{0.25}Ni_{0.75}Fe_2O_4$*	8.3580(3)	583.85(4)	313(3)	0.137(6)
$NiFe_2O_4$	8.3412(4)	580.35(5)	224(2)	0.134(10)
$NiFe_2O_4$*	8.3404(3)	580.18(4)	341(4)	0.109(7)

*coated with starch

Table 2. Refined occupancies (*N*)and cation distributions in tetrahedral (8a) and octahedral (16d) positions of the crystal structures of the investigated ferrites, obtained by the Rietveld method.

	N(Zn)8a	*N*(Ni)8a	*N*(Fe)8a	*N*(Zn)16d	*N*(Ni)16d	*N*(Fe)16d
$ZnFe_2O_4$	0.2455(7)	0.0000(7)	0.0045(7)	0.0045(7)	0.0000(7)	0.4955(7)
$ZnFe_2O_4$*	0.2475(6)	0.0000(6)	0.0037(6)	0.0045(6)	0.0000(6)	0.4932(6)
$Zn_{0.75}Ni_{0.25}Fe_2O_4$	0.1831(6)	0.0066(6)	0.0603(6)	0.0085(6)	0.0618(6)	0.4297(6)
$Zn_{0.75}Ni_{0.25}Fe_2O_4$*	0.1823(7)	0.0059(7)	0.0598(7)	0.0080(7)	0.0623(7)	0.4289(7)
$Zn_{0.5}Ni_{0.5}Fe_2O_4$	0.1201(7)	0.0185(7)	0.1115(7)	0.0050(7)	0.1132(7)	0.3859(7)
$Zn_{0.5}Ni_{0.5}Fe_2O_4$*	0.1193(6)	0.0179(6)	0.1133(6)	0.0063(6)	0.1107(6)	0.3863(6)
$Zn_{0.25}Ni_{0.75}Fe_2O_4$	0.0598(7)	0.0047(7)	0.1913(7)	0.0021(7)	0.1903(7)	0.3087(7)
$Zn_{0.25}Ni_{0.75}Fe_2O_4$*	0.0601(6)	0.0044(6)	0.1901(6)	0.0017(6)	0.1899(6)	0.3069(6)
$NiFe_2O_4$	0.0000(5)	0.0000(5)	0.2498(5)	0.0000(5)	0.2498(5)	0.2502(5)
$NiFe_2O_4$*	0.0000(5)	0.0000(5)	0.2504(5)	0.0000(5)	0.2498(5)	0.2496(5)

*coated with starch

Furthermore, the structural composition of the investigated ferrites was calculated from the results presented in Table 2 and is presented in Table 3, which confirms the agreement between predicted and obtained stoichiometric ratios.

Table 3. Chemical composition of synthesized ferrites deduced from Rietveld refinement and EDS analyses.

	Rietveld method			EDS analysis		
	Zn^{2+}	Ni^{2+}	Fe^{3+}	Zn^{2+}	Ni^{2+}	Fe^{3+}
$ZnFe_2O_4$	1.01	0.00	1.99	1.01	0.00	1.99
$ZnFe_2O_4$*	1.00	0.00	2.00	0.97	0.02	2.01
$Zn_{0.75}Ni_{0.25}Fe_2O_4$	0.76	0.27	1.95	0.76	0.26	2.01
$Zn_{0.75}Ni_{0.25}Fe_2O_4$*	0.77	0.27	1.96	0.74	0.25	1.98
$Zn_{0.5}Ni_{0.5}Fe_2O_4$	0.50	0.51	2.00	0.48	0.54	1.99
$Zn_{0.5}Ni_{0.5}Fe_2O_4$*	0.50	0.53	1.99	0.50	0.46	2.04
$Zn_{0.25}Ni_{0.75}Fe_2O_4$	0.25	0.78	1.99	0.22	0.79	2.01
$Zn_{0.25}Ni_{0.75}Fe_2O_4$*	0.25	0.78	2.00	0.23	0.77	2.02
$NiFe_2O_4$	0.00	1.00	2.00	0.00	0.98	2.02
$NiFe_2O_4$*	0.00	1.00	2.00	0.02	0.99	1.99

*coated with starch

EDS (Table 3) and SEM (Figure 2) analyses were performed to visualize the morphology and nature of the chemical composition of the synthesized magnetic nanoparticles. The results from EDS analyses were in perfect agreement with the chemical composition obtained from XRPD. The slight stoichiometric inconsistencies obtained from the EDS results are due to the sample preparation method. Disagreements in the chemical composition determined by EDS analysis are higher if the investigated samples are not ideally flat, as was the case with the investigated coated powders. From the obtained SEM results (Figure 2), it was clear that the synthesized particles were slightly agglomerated due to their ferrimagnetic nature. However, it is possible to observe particle composition consistency for all of the samples.

According to a group theory consideration, there are 42 vibrational modes that correspond to the spinel structure: A_{1g} (R) + E_g (R) + T_{1g} (in) + 3 T_{2g} (R) + 2 A_{2u} (in) + 2E_u (in) + 4 T_{1u} (IR) + 2 T_{2u} (in), where R and IR represent Raman and infrared active modes, respectively, while in represents inactive modes. Thus, there are four internal IR active bands

that can be found in the following infrared spectral regions: v_1(630–560 cm^{-1}), v_2(525–390 cm^{-1}), v_3(380–335 cm^{-1}), and v_4(300–200 cm^{-1}) [48,49]. The band, v_1, corresponds to intrinsic stretching vibrations of the metal at a tetrahedral site (M_{tetra}–O), whereas the v_2 band is attributed to octahedral metal stretching vibrations (M_{octa}–O). The other two bands can be found in the far-infrared region and are assigned to complex vibrations including both octahedral and tetrahedral sites. A strong band is located at 534 cm^{-1} for the normal spinel structure of $ZnFe_2O_4$, while for the inverse spinel structure of $NiFe_2O_4$, this band lies at 569 cm^{-1} (Figure 3). An increasing trend of the vibrational energy was observed with increasing amount of Ni^{2+} ions in the structure (Figure 3). However, the positions and intensities of the bands depend strongly on the methods and conditions of preparation. A band of weaker intensity that originates from M_{octa}–O vibrations could be found at approximately 450 cm^{-1} for all of the examined species (Figure 3). The band, v_3, appears close to 350 cm^{-1} in all cases, while v_4 is present at a wavenumber lower than 270 cm^{-1}, although sometimes it is difficult to record (Figure 3).

In the spectra of both, pure starch [50, 51] and previously studied coated samples [52], a broad peak approximately 3400 cm^{-1} represents the symmetric vibrations of –O–H groups (Figure 3). The band observed approximately 1100 cm^{-1} can be assigned to O–H bending vibrations. However, the spectra of the coated nanoparticles revealed that this peak split into three close-lying bands (Figure 3). A band observed about 1650 cm^{-1} in the spectra of uncoated ferrites can be attributed to bending vibration of water. At almost the same wavenumber, in the spectra of starch-coated samples the mode of –CH components of starch and ro-vibrational water gas signature are superimposed. An additional band at approximately 2900 cm^{-1}, presenting the C–H stretching modes, appeared in the spectra of the ferrites coated with starch. Moreover, the –CH and $–CH_2$ bending in plane modes of pure starch and starch-coated samples could be found at approximately 1375 and 1455 cm^{-1}. Thus, the

Fourier transform IR (FTIR) spectra confirmed the functionalization by starch of all examined ferrites.

4. Conclusions

Zn-ferrite, Ni^{2+} substituted zinc ferrites and Ni-ferrite magnetic nanoparticles were synthesized *via* the thermal decomposition method and coated with starch.

The XRPD results confirmed the crystalline nature and presence of single phase spinel structure. The unit cell parameter decreased, while the crystallite size increased with decreasing zinc content in the structure. The change of the structure from the normal spinel of $ZnFe_2O_4$ to the inverse spinel of $NiFe_2O_4$ was followed by the microstrain parameter that increased until the composition $Zn_{0.5}Ni_{0.5}Fe_2O_4$ was reached. Further substitution of Zn^{2+} by Ni^{2+} resulted in a reduction in microstrain and relaxation of the structure. According to the SEM and EDS results, the morphology and composition were uniform throughout the samples, corroborating the XRPD data. The FTIR analyses clearly showed the existence of metal oxygen bonds, confirming the presence of the spinel structure. According to the FTIR spectra of the coated samples, additional bands originating from starch appeared, indicating successful functionalization.

The starch coating of nanocrystalline ferrites obtained from acetylacetone complexes presents a very simple and fast way to obtain ferrofluids, opening a broad range of applications.

Acknowledgement

This work was supported by the Serbian Ministry of Education, Science and Technological Development (Grant No. 172035).

References

[1] A. Goldman, Modern Ferrite Technology, second ed., Springer US, New York, 2006.

[2] C. Xiangfeng, J. Dongli, Z. Chenmou, The preparation and gas-sensing properties of $NiFe_2O_4$ nanocubes and nanorods, Sens. Actuator B-Chem. 123 (2007) 793–797.

[3] S.L. Darshane, S.S. Suryavanshi, I.S. Mulla, Nanostructured nickel ferrite: A liquid petroleum gas sensor, Ceram. Int. 35 (2009) 1793–1797.

[4] B.M. Berkovsky, V.F. Medvedev, M.S. Krakov, Magnetic Fluids: Engineering Applications, first ed., Oxford University Press, Oxford, 1993.

[5] M.M. Rashad, O.A. Fouad, Synthesis and characterization of nano-sized nickel ferrites from fly ash for catalytic oxidation of CO, Mater. Chem. Phys. 94 (2005) 365–370.

[6] S. Rana, R.S. Srivastava, M.M. Sorensson, R.D.K. Misra, Synthesis and characterization of nanoparticles with magnetic core and photocatalytic shell: Anatase TiO_2-$NiFe_2O_4$ system, Mater. Sci. Eng. B Solid-State Mater. Adv. Technol. 119 (2005) 144–151.

[7] A.M. Kulkarni, U.V. Desai, K.S. Pandit, M.A. Kulkarni, P.P. Wadgaonkar, Nickel ferrite nanoparticles-hydrogen peroxide: A green catalyst-oxidant combination in chemoselective oxidation of thiols to disulfides and sulfides to sulfoxides, RSC Adv. 4 (2014) 36702–36707.

[8] S. Mukherjee, M.K. Mitra, Effect of nickel ferrite on bismuth ferrite to generate nanocomposite in relation to structure, characterization, magnetic properties and band gap evaluation, Adv. Mater. Lett. 6 (2015) 902–906.

[9] V. Sunny, P. Kurian, P. Mohanan, P.A. Joy, M.R. Anantharaman, A flexible microwave absorber based on nickel ferrite nanocomposite, J. Alloys Compd. 489 (2010) 297–303.

[10] G. Fan, Z. Gu, L. Yang, F. Li, Nanocrystalline zinc ferrite photocatalysts formed using the colloid mill and hydrothermal technique, Chem. Eng. J. 155 (2009) 534–541.

[11] Z. Jia, D. Ren, Y. Liang, R. Zhu, A new strategy for the preparation of porous zinc ferrite nanorods with subsequently light-driven photocatalytic activity, Mater. Lett. 65 (2011) 3116–3119.

[12] X. Li, Y. Hou, Q. Zhao, G. Chen, Synthesis and photoinduced charge-transfer properties of a $ZnFe_2O_4$-sensitized TiO_2 nanotube array electrode, Langmuir. 27 (2011) 3113–3120.

[13] K.J. McDonald, K.-S. Choi, Synthesis and photoelectrochemical properties of $Fe_2O_3/ZnFe_2O_4$ composite photoanodes for use in solar water oxidation, Chem. Mater. 23 (2011) 4863–4869.

[14] G. Lu, S. Li, Hydrogen production by H_2S photodecomposition on $ZnFe_2O_4$ catalyst, Hydrog. Energy. 17 (1992) 767–770.

[15] H. Lv, L. Ma, P. Zeng, D. Ke, T. Peng, Synthesis of floriated $ZnFe_2O_4$ with porous nanorod structures and its photocatalytic hydrogen production under visible light, J. Mater. Chem. 20 (2010) 3665.

[16] H.J. Kim, Y.J. Kim, J.R. Kim, An Integrated LTCC Inductor Embedding NiZn Ferrite, IEEE Trans. Magn. 42 (2006) 2840–2842.

[17] D.L. Zhao, Q. Lv, Z.M. Shen, Fabrication and microwave absorbing properties of Ni-Zn spinel ferrites, J. Alloys Compd. 480 (2009) 634–638.

[18] Y. Hwang, Microwave absorbing properties of NiZn-ferrite synthesized from waste iron oxide catalyst, Mater. Lett. 60 (2006) 3277–3280.

[19] J.Y. Shin, J.H. Oh, The Microwave Absorbing Phenomena of Ferrite Microwave Absorbers, IEEE Trans. Magn. 29 (1993) 3437–3439.

[20] R. Dosoudil, M. Ušáková, J. Franek, J. Sláma, V. Olah, RF electromagnetic wave absorbing properties of ferrite polymer composite materials, J. Magn. Magn. Mater. 304 (2006) 755–757.

[21] G.-P. Yan, L. Robinson, P. Hogg, Magnetic resonance imaging contrast agents: Overview and perspectives, Radiography. 13 (2007) e5–e19.

[22] H. Zhang, L. Li, X.L. Liu, J. Jiao, C.T. Ng, J.B. Yi, Y.E. Luo, B.-H. Bay, L.Y. Zhao, M.L. Peng, N. Gu, H.M. Fan Ultrasmall ferrite nanoparticles synthesized via dynamic simultaneous thermal decomposition for high-performance and multifunctional T_1 magnetic resonance imaging contrast agent, ACS Nano. 11 (2017) 3614–3631.

[23] S.M. Hoque, C. Srivastava, N. Venkatesha, P.S.A. Kumar, K. Chattopadhyay, Superparamagnetic behaviour and T_1, T_2 relaxivity of $ZnFe_2O_4$ nanoparticles for magnetic resonance imaging, Philos. Mag. 93 (2013) 1771–1783.

[24] I. Sharifi, H. Shokrollahi, S. Amiri, Ferrite-based magnetic nanofluids used in hyperthermia applications, J. Magn. Magn. Mater. 324 (2012) 903–915.

[25] A. Hervault, N.T.K. Thanh, Magnetic nanoparticle-based therapeutic agents for thermo-chemotherapy treatment of cancer, Nanoscale. 6 (2014) 11553–11573.

[26] S.A. Shah, M.U. Hashmi, S. Alam, A. Shamim, Magnetic and bioactivity evaluation of ferrimagnetic $ZnFe_2O_4$ containing glass ceramics for the hyperthermia treatment of cancer, J. Magn. Magn. Mater. 322 (2010) 375–381.

[27] S.M. Hoque, M.S. Hossain, S. Choudhury, S. Akhter, F. Hyder, Synthesis and characterization of $ZnFe_2O_4$ nanoparticles and its biomedical applications, Mater. Lett. 162 (2016) 60–63.

[28] N.T.K. Thanh, Magnetic Nanoparticles: From Fabrication to Clinical Applications, first edition, CRC Press Taylor & Francis Group, Boca Raton, London, New York, 2012.

[29] C. Sun, J.S.H. Lee, M. Zhang, Magnetic nanoparticles in MR imaging and drug delivery, Adv. Drug Deliv. Rev. 60 (2008) 1252–1265.

[30] X. Li, J. Wei, K.E. Aifantis, Y. Fan, Q. Feng, F.-Z. Cui, F. Watari, Current investigations into magnetic nanoparticles for biomedical applications, J. Biomed. Mater. Res. - Part A. 104 (2016) 1285–1296.

[31] G. Chen, I. Roy, C. Yang, P.N. Prasad, Nanochemistry and nanomedicine for nanoparticle-based diagnostics and therapy, Chem. Rev. 116 (2016) 2826–2885.

[32] A.H. Lu, E.L. Salabas, F. Schüth, Magnetic nanoparticles: Synthesis, protection, functionalization, and application, Angew. Chemie - Int. Ed. 46 (2007) 1222–1244.

[33] A. Hajalilou, S.A. Mazlan, A review on preparation techniques for synthesis of nanocrystalline soft magnetic ferrites and investigation on the effects of microstructure features on magnetic properties, Appl. Phys. A Mater. Sci. Process. 122 (2016) 1–15.

[34] S. Jauhar, J. Kaur, A. Goyal, S. Singhal, Tuning the properties of cobalt ferrite: A road towards diverse applications, RSC Adv. 6 (2016) 97694–97719.

[35] I.A. Fernandes de Medeiros, A.L. Lopes-Moriyama, C.P. de Souza, Effect of synthesis parameters on the size of cobalt ferrite crystallite, Ceram. Int. 43 (2017) 3962–3969.

[36] M. Vučinić-Vasić, B. Antić, A. Kremenović, A.S. Nikolić, M. Stoiljković, N. Bibić, V. Spasojević, Ph. Colomban, Zn,Ni ferrite/NiO nanocomposite powder obtained from acetylacetonato complexes, Nanotechnology. 17 (2006) 4877–4884.

[37] S. Hazra, N.N. Ghosh, Preparation of nanoferrites and their applications, J. Nanosci. Nanotechnol. 14 (2014) 1983–2000.

[38] B. Antić, A. Kremenović, N. Jović, M.B. Pavlović, Č. Jovalekić, A.S. Nikolić, G.F. Goya, C. Weidenthaler , Magnetization enhancement and cation valences in nonstoichiometric $(Mn,Fe)_{3-\delta}O_4$ nanoparticles, J. Appl. Phys. 111 (2012) 074309(6).

[39] B. Antić, A. Kremenović, A.S. Nikolić, M. Stoiljković, Cation distribution and size-strain microstructure analysis in ultrafine Zn-Mn ferrites obtained from acetylacetonato complexes, J. Phys. Chem. B. 108 (2004) 12646–12651.

[40] A.S. Nikolić, Z.B. Maričić, T.J. Sabo, M. Kuraica, S. Djurić, N. Juranić, Method for the preparation of Ni-ferrites from β-diketonato complex compounds, J. Serbian Chem. Soc. 64 (1999) 297–302.

[41] G. Goloverda, B. Jackson, C. Kidd, V. Kolesnichenko, Synthesis of ultrasmall magnetic iron oxide nanoparticles and study of their colloid and surface chemistry, J. Magn. Magn. Mater. 321 (2009) 1372–1376.

[42] A.K. Gupta, M. Gupta, Synthesis and surface engineering of iron oxide nanoparticles for biomedical applications, Biomaterials. 26 (2005) 3995–4021.

[43] R. Tadmor, R.E. Rosensweig, J. Frey, J. Klein, Resolving the puzzle of ferrofluid dispersants, Langmuir. 16 (2000) 9117–9120.

[44] A.R. Devi, J.A. Chelvane, P.K. Prabhakar, B. Venkateswarlu, M. Doble, B.S. Murty, Influence of surfactant variation on effective anisotropy and magnetic properties of mechanically milled magnetite nanoparticles and their biocompatibility, IEEE Trans. Magn. 50 (2014) 10–13.

[45] R.W. Cheary, A. Coelho, Fundamental parameters approach to X-ray line-profile fitting, J. Appl. Crystallogr. 25 (1992) 109–121.

[46] I.H. Gul, W. Ahmed, A. Maqsood, Electrical and magnetic characterization of nanocrystalline Ni-Zn ferrite synthesis by co-precipitation route, J. Magn. Magn. Mater. 320 (2008) 270–275.

[47] G.S. Shahane, A. Kumar, M. Arora, R.P. Pant, K. Lal, Synthesis and characterization of Ni-Zn ferrite nanoparticles, J. Magn. Magn. Mater. 322 (2010) 1015–1019.

[48] K.V.S. Badarinath, The far infrared spectra of $MgAl_{2-x}Fe_xO_4$ spinel, Phys. Stat. Sol. 91 (1985) K19–K22.

[49] D. Ravinder, Far-infrared spectral studies of mixed lithium–zinc ferrites, Mater. Lett. (1999) 205–208.

[50] F. J. Warren, M. J. Gidley, B. M. Flanagan, Infrared spectroscopy as a tool to characterise starch ordered structure—a joint FTIR–ATR, NMR, XRD and DSC study, Carbohydr Polym. 139 (2016) 35–42

[51] A. Galat, Study of the Raman scattering and infrared absorption spectra of branched polysaccharidies, Acta Biochim Pol. 27 (1980) 135-142

[52] D.-H. Kim, K.-N. Kim, K.-M. Kim, Y.-K. Lee, Targeting to carcinoma cells with chitosan- and starch-coated magnetic nanoparticles for magnetic hyperthermia, J Biomed Mater Res A 88A (2009) 1-11

Figure 1. Collected XRPD patterns of synthesized a) uncoated and b) starch-coated Zn-ferrite, Ni-ferrite and mixed Ni–Zn ferrites.

Figure 2. SEM analysis of the synthesized ferrites; *samples coated with starch.

Figure 3. FTIR spectra of the synthesized ferrites.

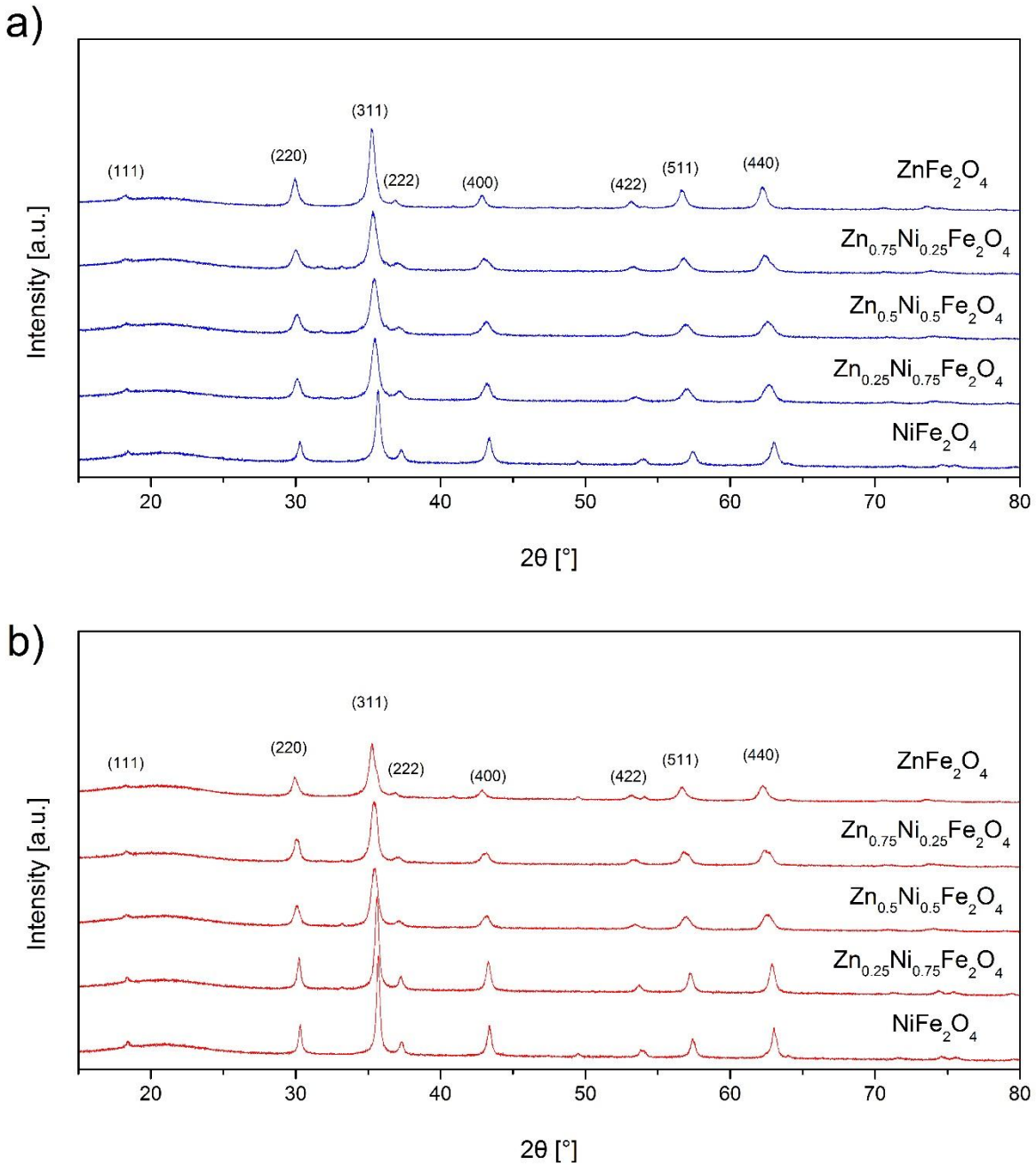

Figure 1. Collected XRPD patterns of synthesized a) uncoated and b) starch-coated Zn-ferrite, Ni-ferrite and mixed Ni–Zn ferrites.

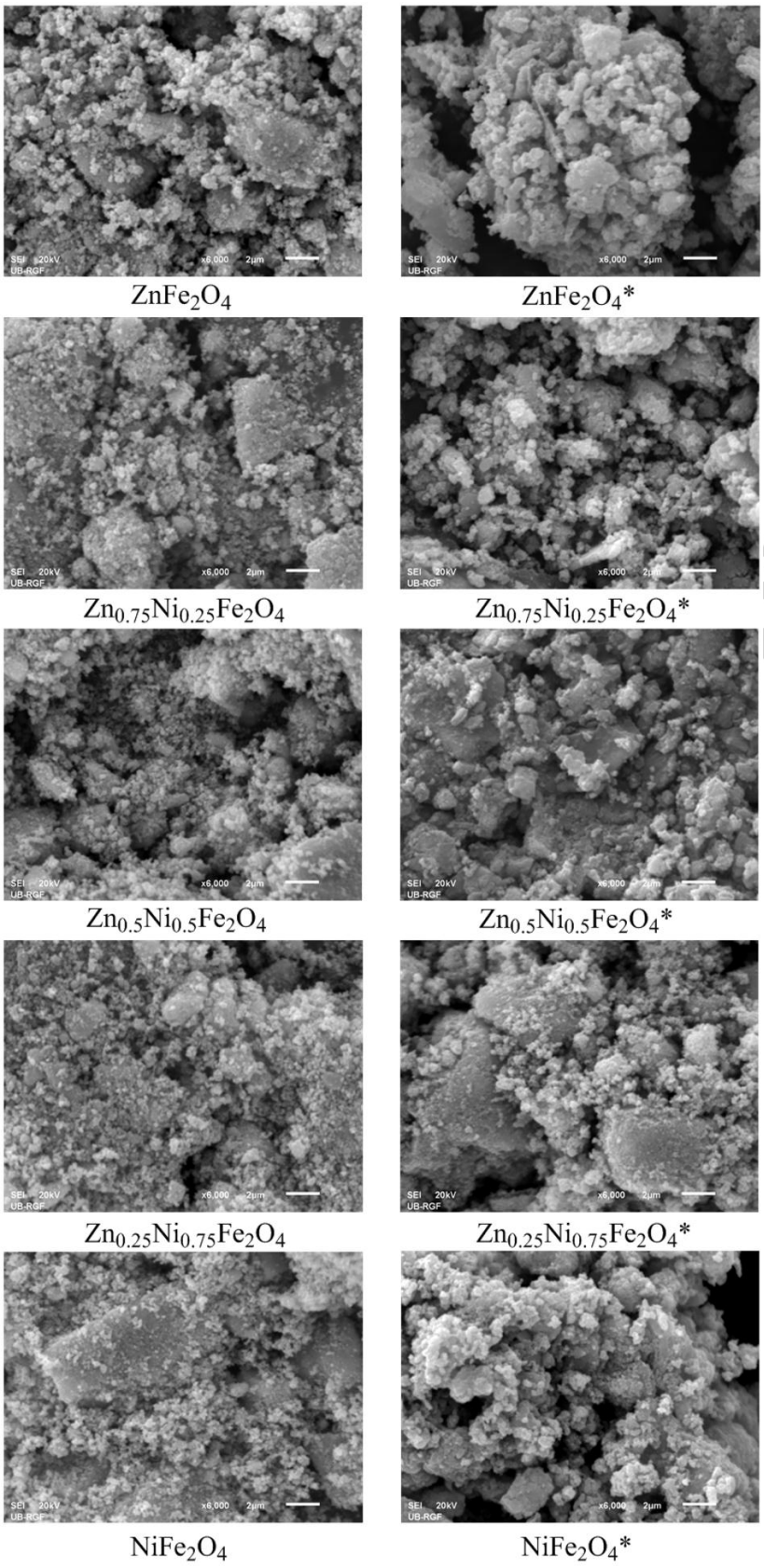

Figure 2. SEM analysis of the synthesized ferrites; *samples coated with starch.

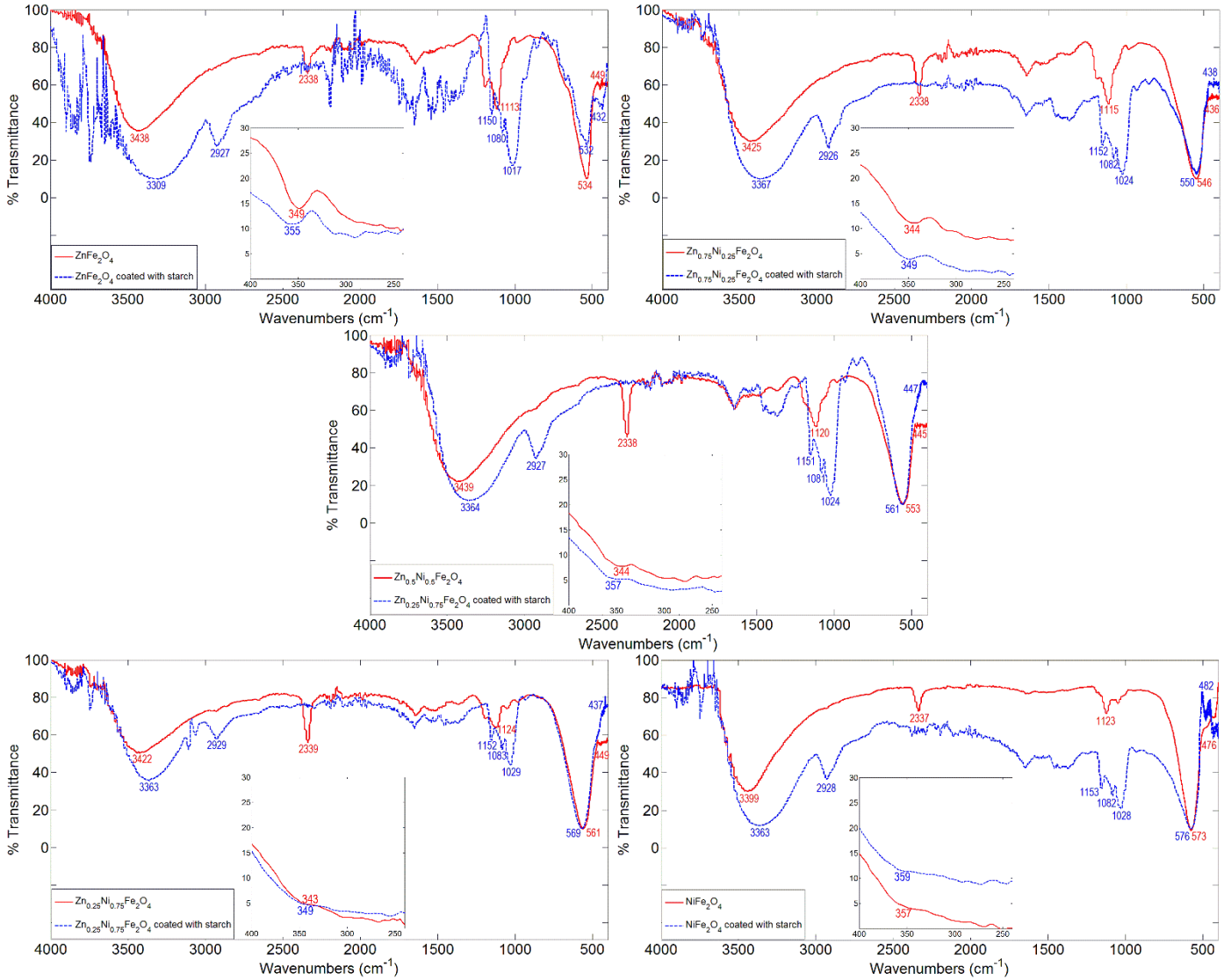

Figure 3. FTIR spectra of the synthesized ferrites.